Photodriven Self-Excited Hydrogel Oscillators

Chen Xuan,[1,†,‡] Yu Zhou,[1,‡] Yusen Zhao,[2] Ximin He,[2] and Lihua Jin[1,*]

[1]*Department of Mechanical and Aerospace Engineering, University of California, Los Angeles, 90095, USA*
[2]*Department of Materials Science and Engineering, University of California, Los Angeles, 90095, USA*

Stimuli-responsive materials are designed for self-sustained soft robots. Using a photothermally responsive hydrogel cantilever as a model system, this paper investigates the mechanism and energy flow in self-excited oscillation under a constant light source. Based on an analytical model, we show that a periodic photomoment, produced by nonuniform water concentration across the cantilever's thickness driven by diffusion, is imposed on the cantilever by the ever-switching light incidence between the top and bottom surfaces. The synergy between the photomoment and oscillation ensures positive work input to the cantilever when the diffusion timescale is comparable to the period of free oscillation. When the input energy is higher than the damping energy, the oscillation amplitude increases, while, when the input energy is lower, the amplitude decreases. Based on dimensional energy analysis, we determine the stable oscillation amplitude and construct phase diagrams for the increase and decrease of the oscillation amplitude, which are further confirmed experimentally. A mass-spring-damper system subjected to a displacement-dependent excitation force is developed to investigate the features in generalized self-excited oscillating systems. This work lays a solid foundation for understanding self-excited oscillation and provides design guidelines for self-sustainable soft robots.

I. INTRODUCTION

Stimuli-responsive materials can alter their shapes, volumes, or functions in response to external stimuli, such as heat, light, chemical, or electrical fields [1]. Building soft robots with stimuli-responsive materials is the most promising strategy to achieve their miniaturization and untethered locomotion. However, to accomplish sustainable motions of such soft robots, the complex control of external stimuli is usually essential [2–6]. An emergent trend is designing self-sustainable soft robots that can maintain motions under simple or constant external stimuli through the sophisticated interaction between stimuli-responsive materials and external stimuli [7–15].

One of the most useful self-sustainable motions is self-excited oscillation, i.e., autonomous oscillation of stimuli-responsive materials without artificially switching *on* and *off* external stimuli [8,16–21]. It is especially inspired by biological rhythms, i.e., oscillatory changes of chemical or mechanical functions, in living organisms; examples include circadian clocks and heartbeats.

A hydrogel with its polymer network undergoing a nonequilibrium oscillatory reaction, such as the Belousov-Zhabotinsky reaction, is capable of autonomous swelling and deswelling cycles [22,23]. A humidity-responsive material in a humidity gradient can bend and oscillate [24]. An alternative strategy is to utilize the fact that the deformation of photoresponsive materials can alter or even block light incidence [13,25], which drives the recovery of deformation, inducing a cyclic response. Autonomous oscillation [16,26–29] and continuous-wave propagation [30] have been achieved and modeled [7,31–33] in photoresponsive liquid-crystal elastomers and hydrogels under constant light radiation. Although the process of the self-excited oscillation is relatively intuitive, it is not clear how the autonomous oscillation is maintained through the sophisticated interaction and energy flow between stimuli-responsive materials and external stimuli, and how material and geometric parameters govern the stable oscillation behavior.

Here, we investigate a photodriven self-excited hydrogel oscillator that can autonomously vibrate under constant light and determine its stable oscillation behavior by examining its energy flow (Fig. 1). A hydrogel is a polymer network dispersed in water. In a photothermally responsive hydrogel, heating due to photoabsorption can trigger a chemical potential increase of the water molecules, and induce deswelling of the hydrogel.

─────────
*lihuajin@seas.ucla.edu
†Current address: Department of Foundational Mathematics, School of Science, Xi'an Jiaotong-Liverpool University, Suzhou 215123, China
‡C. Xuan and Y. Zhou contributed equally to this work.

When the photothermally responsive hydrogel cantilever [Fig. 1(a)] deviates from its horizontal rest position, the light shines on one of its surfaces, driving water molecules to diffuse out of the hydrogel and forming a concentration gradient, which produces a moment to bend the cantilever towards the opposite direction. Since the moment is photoinduced, we simply call it photomoment. Once the cantilever deflects beyond the rest position, the light relocates onto the opposite surface, creating an additional negative photomoment to bend the cantilever back to the original side. This process can go on periodically under an ever-switching photomoment. Our system falls into the categories of nonsmooth piecewise systems and nonharmonic dynamically shifted oscillators [34–37]. We analyze the work input into the hydrogel through its sophisticated interaction with constant light and the damping energy output to external water. Balance of the work input and damping energy will allow us to determine the stable oscillation amplitude, which is governed by several dimensionless material and geometric parameters. We theoretically and experimentally show that oscillation with a different amplitude will autonomously increase or decrease its amplitude until reaching a stable value. A simplified mass-spring-damper model is further developed to manifest the mechanism and energy flow of generalized self-excited oscillating systems.

II. THEORY FOR SELF-EXCITED HYDROGEL OSCILLATORS

We model the vibration of a hydrogel cantilever of length L and thickness h in water triggered by constant light radiation in the axial direction [Fig. 1(a)]. The cantilever is assumed to undergo a small deflection, $w(x, t)$, with respect to its equilibrium free swelling state, as a function of coordinate x and time t, governed by

$$\rho A \frac{\partial^2 w}{\partial t^2} + c \frac{\partial w}{\partial t} + EI \frac{\partial^4 w}{\partial x^4} = EI \frac{\partial^2 (1/R_{\mathrm{ph}})}{\partial x^2}, \quad (1)$$

with density ρ, cross-section area A, Young's modulus E, and area moment of inertia I. The second term assumes that the damping force on a unit length of the hydrogel is proportional to the deflection velocity, with damping coefficient c, due to the drag from the water. With the left end clamped and the right end free, the boundary conditions are

$$w(0, t) = \frac{\partial w}{\partial x}(0, t) = 0, \ \frac{\partial^2 w}{\partial x^2}(L, t) = \frac{\partial^3 w}{\partial x^3}(L, t) = 0. \quad (2)$$

The term on the right-hand side of Eq. (1) is the distributed load produced by the photomoment, EI/R_{ph}, where R_{ph} is the spontaneous radius of curvature in the illuminated region, $x \in [0, d_{\mathrm{ph}}]$, arising from a gradient of photodriven

deformation through the thickness. This causes local bending of the beam in the region $x \in [0, d_{\mathrm{ph}}]$. The spontaneous curvature can be obtained as (Appendix A)

$$1/R_{\mathrm{ph}} = -\int_A \varepsilon_{\mathrm{ph}}(z) z \, \mathrm{d}A/I, \quad (3)$$

where $\boldsymbol{\varepsilon}_{\mathrm{ph}}(z) = \mathrm{diag}[\varepsilon_{\mathrm{ph}}(z), \varepsilon_{\mathrm{ph}}(z), \varepsilon_{\mathrm{ph}}(z)]$ is the spontaneous photostrain at position z induced by photodriven diffusion. Assuming the hydrogel undergoes pure bending with respect to the nonirradiated state, photostrain is related to the water concentration, C, through $\varepsilon_{\mathrm{ph}}(z) \doteq \{[\Omega C(z) + 1]/(\Omega C_0 + 1) - 1\}/3$, where C_0 is the water concentration in the hydrogel when the hydrogel is in equilibrium with pure water without radiation.

We model the photothermally driven water migration as a one-dimensional diffusion problem along the thickness [38,39],

$$\frac{\partial C}{\partial t} = \frac{D}{k_B T} \frac{\partial}{\partial z} \left(\frac{C}{\lambda_z^2} \frac{\partial \mu}{\partial z} \right), \quad (4)$$

where λ_z is the stretch ratio of the hydrogel in the current state with respect to its nonradiated equilibrium state, μ is the chemical potential of water molecules in the hydrogel (defined in Appendix A), and D is the diffusivity of water molecules in the hydrogel. Although it should be noted that hydrogels may have different diffusion kinetics for swelling and deswelling [40], here, according to our theory, we just use Eq. (4) to describe both swelling and deswelling. To capture the fact that water molecules diffuse out of the hydrogel through the illuminated surface, we simply assume that light changes the chemical potential of water molecules on the illuminated boundary, i.e., apply $\mu = -\mu_{\mathrm{ph}} < 0$ on the illuminated surface and $\mu = 0$ on the nonilluminated surface.

The photoinduced bending curvature, Eq. (3), produces a photomoment in the region $x \in [0, d_{\mathrm{ph}}]$ in Eq. (1). In the meantime, $\varepsilon_{\mathrm{ph}}(z)$ is governed by diffusion Eq. (4). Solving Eqs. (1) and (4) together, we can fully determine the spatiotemporal response of the photodriven hydrogel oscillator. Both Eqs. (1) and (4) are solved by the forward-time central-space finite-difference method. The solution of Eq. (4) will enable one to calculate the spontaneous radius of curvature from Eq. (3) as an input to the right-hand side of Eq. (1) at every time step. In such a coupling process between the beam vibration and water diffusion, there are three timescales, the viscous relaxation timescale $t_c = \rho A/c$, the inertia time scale $t_{\mathrm{i}} = \sqrt{\rho A L^4 / EI}$, and the diffusion timescale $t_d = h^2/D$, arising from Eqs. (1) and (4), which lead to two timescale ratios, t_i/t_c and t_i/t_d. Clearly, the timescale ratio t_i/t_c represents the normalized damping factor, indicating how large the damping force is compared to the inertia force, and t_i/t_d represents
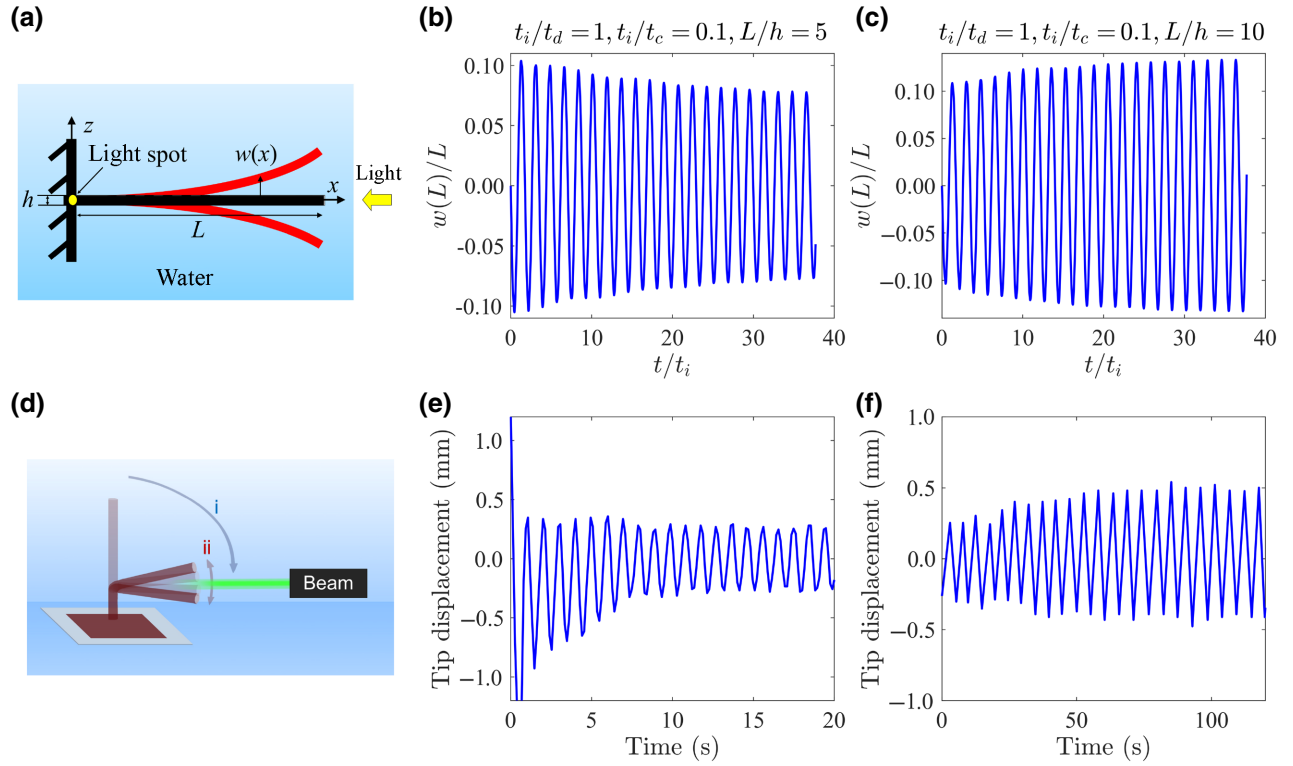
FIG. 1. (a) Schematic of self-excited oscillation of a hydrogel cantilever in response to constant light radiation. (b),(c) Time response of the cantilever's tip displacement for different length-to-thickness ratios. Tip amplitude decreases with time for $L/h = 5$ and increases for $L/h = 10$. (d) Schematics of the experimental setup for self-excited oscillation of a photothermally responsive hydrogel. Time response of the tip displacement of (e) thick ($h = 0.9$ mm, $L/h = 18.9$) and (f) thin ($h = 0.56$ mm, $L/h = 30.4$) cantilevers of length $L = 17$ mm.

the normalized diffusivity, indicating how fast water diffuses compared with the vibration velocity. We show that these two normalized parameters can greatly influence the vibration behavior.

III. RESULTS

A. Amplitude increase and decrease

A cantilever starting from the horizontal position with an initial velocity, $v_0(x) = \dot{\theta}_0 x$, vibrates under inertia and radiation. Following our previous work [7], parameters for all simulations are set as $d_{\mathrm{ph}}/L = 1/20$, $N\Omega = 10^{-3}$, $\chi = 0.3$, $\mu_{\mathrm{ph}}/k_B T = 3 \times 10^{-4}$, $v_0(L)t_i/L = -1/3$, and $L/h = 10$, unless otherwise stated. Two types of vibration behavior are observed: the amplitude of deflection decreases [Fig. 1(b) and Movie S1 within the Supplemental Material [41]] or increases [Fig. 1(c) and Movie S2 within the Supplemental Material [41]] over time and saturates when time is long enough for both cases. Although light radiation is constant, it passively switches its incident spot piecewise between the top and bottom surfaces in the same period as the oscillation, forming a photodriven self-excited oscillation. Whether the amplitude decreases or increases depends on different parameters, including

the normalized damping factor, the normalized diffusivity, the geometry, the radiation-induced chemical potential decrease, and the initial velocity. As a demonstration, we vary only the length-to-thickness ratio [$L/h = 5$ for Fig. 1(b) and $L/h = 10$ for Fig. 1(c)], and detailed phase diagrams for the increase and decrease of the oscillation amplitude will be provided later. The angular frequencies in both cases are close to the classical limit of cantilever vibration, $3.5/t_i$, indicating that the bending shape is roughly in the first mode of cantilever vibration [Figs. 1(b) and 1(c)].

B. Experiments

To experimentally verify the existence of both cases of amplitude increasing and decreasing, we demonstrate oscillation of a poly(N-isopropylacrylamide) (PNIPAAm) hydrogel [Fig. 1(d)], where gold nanoparticles (AuNPs) are added to incorporate the photothermal effect [7]. To fabricate hydrogel pillars, the AuNPs-PNIPAAm precursor solution is prepared with 40-wt % NIPAAM monomer, 1.5-wt % N,N'-methylenebis(acrylamide) (BIS), 0.5-vol % Darocur 1173, and 0.5-wt % AuNPs in dimethyl sulfoxide, and then cured in a poly(dimethylsiloxane) (PDMS) mold under UV light for 80 s. Details of

the synthesis and characterization of the gold nanoparticles can be found in the literature [7]. Pillars with a circular cross section of two different diameters are fabricated. The as-prepared diameters are 0.71 and 0.50 mm, and the corresponding equilibrium swelling diameters are 0.9 and 0.56 mm, respectively. After the hydrogels reach equilibrium in water, the Young's modulus is measured to be 6.3 kPa. Upon exposure to a green laser (532 nm and $\geq$200 mW, with a beam diameter of 1 mm), the hydrogel is heated on the front surface due to photoabsorption of the gold nanoparticles. Once the temperature reaches the lower critical solution temperature of PNIPAAm (approximately 32 °C), water molecules diffuse out, which creates a concentration gradient in the thickness direction, and bends the initially vertical hydrogel pillar to the horizontal direction, followed by autonomous oscillation of the effective cantilever about the horizontal plane [Fig. 1(d)]. For a hydrogel cantilever of length $L = 17$ mm, the amplitude decays over time when the diameter is $h = 0.9$ mm [$L/h = 18.9$, Fig. 1(e) and Movie S3 within the Supplemental Material [41]], while the amplitude grows over time when the diameter is $h = 0.56$ mm [$L/h = 30.4$, Fig. 1(f) and Movie S4 within the Supplemental Material [41]].

It should be noted that there are some differences between the theory and the experiments. Our goal is to build a generic framework to study the self-excitation of hydrogel beam structures and understand its mechanism, while experiments are a demonstration of the self-excitation phenomenon. In the experiments, the hydrogel pillar is bent from the initially vertical position to the horizontal direction, while a horizonal hydrogel cantilever is modeled in the theory. The experimental setup gives a substantial initial speed of the hydrogel beam as it hits the horizontal position. Our theory starts from a horizontal position with an input initial speed, so the theory and experiments are consistent. We skip the initial process from the vertical to horizontal position in the theory, since it is not the essential part we are interested in. In experiments, when the hydrogel is at the largest downward deflection, the light is almost blocked by its tip, leading to different boundary conditions between the top and bottom surfaces. Ideally, when the beam is thin enough, light can shine on the corner of the top surface, resulting in better agreement between experiment and theory. On the other hand, our theory is also capable of modeling the case when light is blocked by the tip of the hydrogel by setting the chemical-potential boundary condition of the top surface to be always zero.

C. Without damping

To understand the requirements for a self-excited oscillation, we first investigate the effect of the normalized diffusivity for an ideal scenario without damping. When the

diffusion timescale is comparable to the inertia timescale [$t_i/t_d = 1$ in Fig. 2(a)], the vibration amplitude increases over time. The amplitude grows without saturation due to a lack of damping. The photocurvature changes in a periodic manner, but with a phase lag of about $\pi/2$ with respect to the tip deflection due to the nonequilibrium diffusion process [Fig. 2(a)]. The photocurvature is a consequence of an inhomogeneous distribution of water concentration C and photostrain ε_{ph} through the thickness direction [Fig. 2(c)]. The work done to the cantilever by light over time t can be calculated as $W_l(t) = \int_0^t EI\dot{\theta}/R_{ph}d\tau$, where $\dot{\theta}$ is the rate of change of the angle at $x = d_{ph}$ [Fig. 2(b)]. The irregular time response of $\dot{\theta}$ is due to vibration with multiple modes. When the cantilever strokes downward from the horizontal position, the radiation spot leaves the bottom surface and moves onto the top surface, and the photocurvature reaches the valley [insets of Fig. 2(a)]. The radiation on the top surface decreases the water concentration in its vicinity and increases the photocurvature. Due to diffusion, it takes some time (less than a quarter period) for the curvature to reach zero. Considering that $\dot{\theta}$ is negative, the photomoment does positive and negative work to the cantilever, before and after the curvature reaches zero, respectively [insets of Figs. 2(a) and 2(b)]. After the tip deflection reaches its valley, $\dot{\theta}$ becomes positive and the photomoment does positive work to the cantilever again. When the cantilever hits the horizontal line, the irradiated spot switches to the bottom surface, and the photocurvature reaches its peak. Therefore, within the half-vibration period, the total work done to the cantilever first increases, then decreases, and increases again [insets of Fig. 2(b)]; the total work follows a similar trend within the next half period. Due to the synergy of the photomoment and the rate of change of the bending angle, the net work done to the system over a period is positive, which leads to the increase of the deflection amplitude. When the cantilever just starts to vibrate, the water concentration decreases only in the outer layer in response to radiation [the black curve in Fig. 2(c)]. In the later cycles, the outer layer on the side illuminated shrinks more, and the outer layer without radiation partially reswells. The shrinkage zone goes deeper and deeper into the cantilever [the red curve in Fig. 2(c)] and eventually saturates.

When diffusion is much slower than vibration, the beam vibrates periodically with a fixed amplitude [$t_i/t_d = 0.0001$ in Fig. 2(d)], as the photomoment built up on a timescale of inertia is so small that the work done to the cantilever is negligible. When diffusion is much faster than vibration, the photocurvature acts like a step-function excitation (Appendix B). Therefore, once the cantilever goes below the horizontal line, photocurvature immediately becomes positive, so positive and negative work cancel each other out and vice versa. Also, since diffusion is fast, it perturbs the regular bending mode of the cantilever,
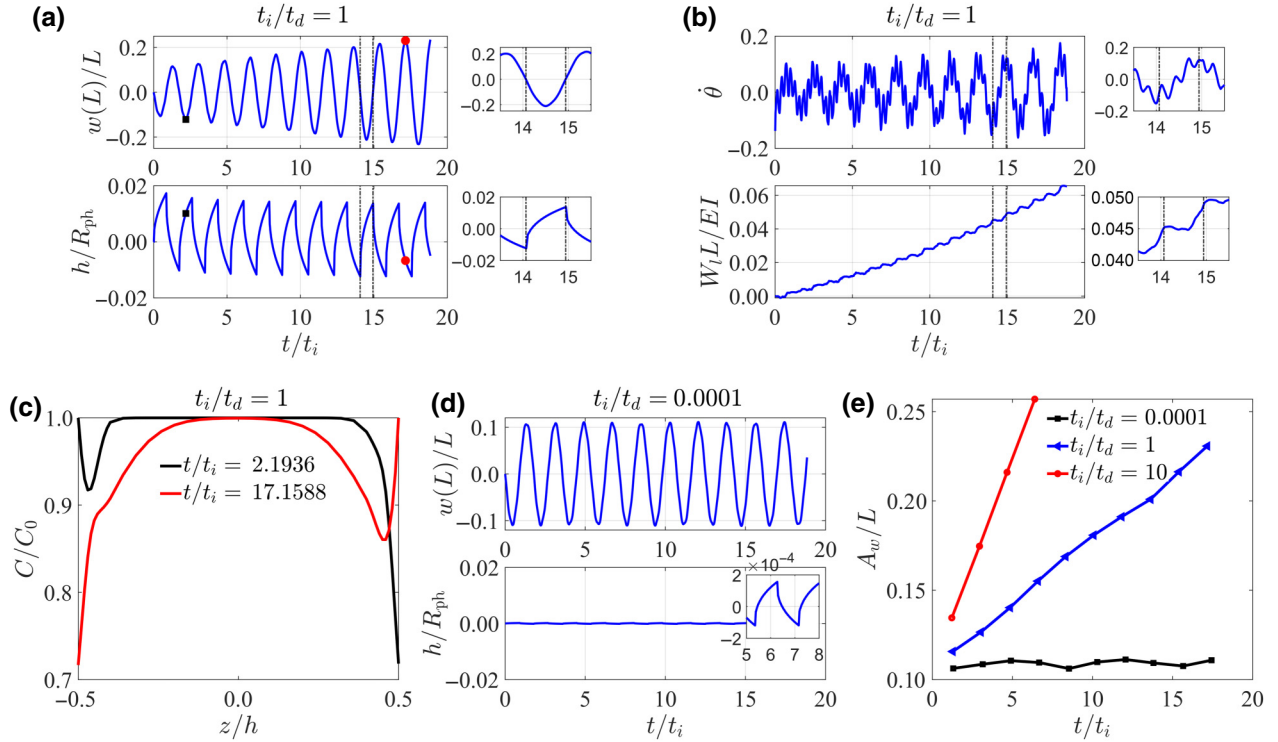
FIG. 2. (a),(d) Time response of the cantilever's tip displacement, $w(L)/L$, and photocurvature, h/R_{ph}, for different normalized diffusivities, $t_i/t_d = 1$, 0.0001, respectively. (b) Time response of the rate of change of the bending angle, $\dot{\theta}$, at $x = d_{ph}$ and the work done to the cantilever, $W_l L/EI$. (c) Water-concentration depth profiles at different times, $t/t_i = 2.19$ and $t/t_i = 17.15$, corresponding to the valley and peak of tip displacements indicated by the black square and red circle in (a). (e) Amplitude of tip displacement as a function to time for different t_i/t_d.

leading to excitation composed of multiple bending modes other than the first mode. In this case, the cantilever will block light, violating the assumption that the light shines in the region $x \in [0, d_{ph}]$. Therefore, in our later study, normalized diffusivity will be limited to less than 20. Below this limit, a higher normalized diffusivity leads to a larger photomoment and higher work input, which increases the amplitude of deflection faster [Fig. 2(e)].

D. With damping

Next, we consider self-excited hydrogel oscillators subjected to damping. Given different normalized damping factors, the tip deflection amplitude, A_w, either increases or decreases over time and then saturates [Fig. 3(a)]; the saturated value is called the stable amplitude. As the normalized damping factor increases, the stable amplitude decreases [Fig. 3(a)], and the diminishing amplitude causes the angular frequency, $\omega = 2\pi/T_p$, to increase [Fig. 3(b)], where T_p is the period of the vibration. The normalized diffusivities, t_i/t_d, within certain range show little effect on the vibration frequency [Fig. 3(b)]. If the normalized diffusivity is further increased, i.e., $t_i/t_d = 100\,000$, the vibration frequency increases (Appendix B). The energy loss due to damping over time, t, can be calculated as

$W_c(t) = \int_0^t \int_0^L c\dot{w}^2 dx d\tau$. As a result, when the cantilever just starts to vibrate, the system with a larger normalized damping factor exhibits higher energy dissipation. However, when the vibration reaches the steady state, it has a lower energy dissipation due to a lower stable amplitude [Fig. 3(c)], implying that energy loss is influenced by both the vibration amplitude and damping factor.

E. Scaling analysis for energy flow

We further investigate the effect of other parameters on self-excited oscillation and conduct scaling analysis for the work input and energy dissipation to construct a phase diagram for the increase and decrease of the oscillation amplitude (Figs. 4 and 5). The radiation does work $W_{lp} = \int_0^{T_p} EI\dot{\theta}/R_{ph} dt$ to the cantilever over a period. Since the bending angle scales as $\theta \sim A_w/L$, the work done to the cantilever can be rewritten as $W_{lp} \sim EIA_w/(R_{ph}L)$. Using Eq. (3) and assuming a linear distribution of spontaneous photostrain along the thickness direction, we find that the spontaneous radius of curvature scales with the square of the thickness, $R_{ph} \sim h^2$, and is inversely proportional to the diffusion thickness, $\sqrt{DT_p}$, and nonlinearly depends on the photochemical potential, $\mu_{ph}/k_B T$ (Appendix C). Therefore, the work per period can be further rewritten as
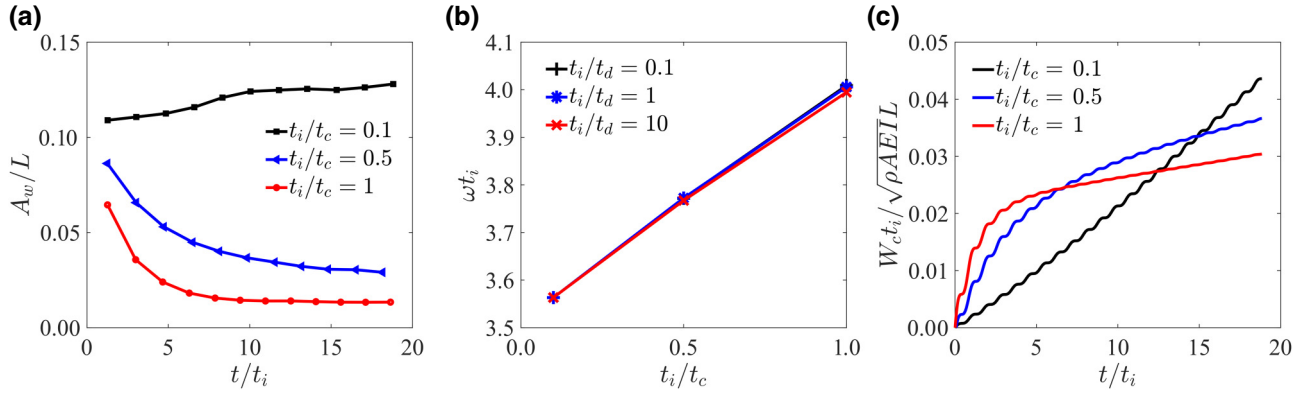
FIG. 3. (a) Time response of the amplitude of tip displacement for different normalized damping factors. (b) Influence of the normalized damping factor and diffusivity on the cantilever oscillation frequency. (c) Time response of energy loss for different damping factors.

$W_{lp} \sim f\,(\mu_{\mathrm{ph}}/k_B T)EIA_w\sqrt{DT_p}/Lh^2$, with f as an increasing function of $\mu_{\mathrm{ph}}/k_B T$. As Fig. 3(b) shows, the period T_p can be further expressed as $t_i/g(t_i/t_d, t_i/t_c)$, where g is a weak function of t_i/t_d and t_i/t_c, and we can treat it as a constant. In combination with the diffusion timescale, $t_d = h^2/D$, we have

$$W_{lp} \sim f\,(\mu_{\mathrm{ph}}/k_B T)(1/h)\left(EI\sqrt{t_i/t_d}\right)(A_w/L). \quad (5)$$

In the meantime, the energy loss of the cantilever over a period due to damping can be calculated by $W_{cp} \sim \int_0^{T_p}\int_0^L c\dot{w}^2 dx dt$, where deflection w scales with tip amplitude A_w, so we have

$$W_{cp} \sim cLA_w^2/T_p \sim (1/t_i)(cL^3)(A_w/L)^2. \quad (6)$$

Consistent with the classical self-excited oscillation [42], our numerical results indeed show that, under various damping factors and geometric parameters, the normalized work done to the cantilever, $W_{lp}h/(EI\sqrt{t_i/t_d})$, is proportional to the normalized tip amplitude, A_w/L, with fitted slope $k_l = 3.793 \times 10^{-3}$ [Fig. 4(a)], and the normalized damping energy, $W_{cp}t_i/cL^3$, is proportional to the square of the normalized tip amplitude $(A_w/L)^2$ with fitted slope $k_c = 2.895$ [Fig. 4(b)]. To further compare the work input and energy dissipation within a period, we normalize both of them by cL^3/t_i, which are equal to $k_l(L/h)(A_w/L)\sqrt{t_i/t_d}/(t_i/t_c)$ and $k_c(A_w/L)^2$, respectively, and are plotted as functions of A_w/L [Fig. 4(c)]. The results are based on the parameters $t_i/t_c = 1$, $t_i/t_d = 1$, and $L/h = 10$, which are not used for fitting in Figs. 4(a) and 4(b). The intersection of the two curves determines the stable amplitude, and it agrees well with the results obtained in Fig. 3(a). By using $W_{lp} = W_{cp}$, we obtain the scaling of

the stable amplitude:

$$A_w/L \sim f\,(\mu_{\mathrm{ph}}/k_B T)\frac{L}{h}\frac{\sqrt{t_i/t_d}}{t_i/t_c}$$
$$\sim f\,(\mu_{\mathrm{ph}}/k_B T)Ah^{-\frac{3}{2}}\rho^{\frac{3}{4}}E^{\frac{1}{4}}D^{\frac{1}{2}}C^{-1}. \quad (7)$$

Clearly, a higher normalized diffusivity t_i/t_d, higher length-to-thickness ratio L/h, or lower normalized damping factor t_i/t_c increases the normalized work $W_{lp}t_i/cL^3$, and therefore, increases the stable amplitude [Fig. 4(c)].

Depending on whether the initial amplitude, A_0, is smaller or larger than A_w, the amplitude increases or decreases to reach A_w. Since the initial amplitude scales with the initial velocity, $A_0/L \sim v_0(L)T_p/L \sim v_0(L)t_i/L$, the boundary between amplitude increase and decrease, $A_0/L = A_w/L$, gives

$$v_0(L)t_i/L \sim f\,(\mu_{\mathrm{ph}}/k_B T)\frac{L}{h}\frac{\sqrt{t_i/t_d}}{t_i/t_c}. \quad (8)$$

The decisive dimensionless material and geometric parameters for the phase boundary are $\mu_{\mathrm{ph}}/k_B T$, $v_0(L)t_i/L$, t_i/t_d, t_i/t_c, and L/h. Consistent with Eq. (8), the numerical results show linear boundaries between the amplitude increasing and decreasing regions in the phase plane of t_c/t_i and $v_0(L)t_i/L$ [Fig. 4(d)], the phase plane of t_i/t_c and $\sqrt{t_i/t_d}$ [Fig. 4(e)], and the phase plane of t_i/t_c and L/h [Fig. 4(f)]. Figure 4(g) shows a nonlinear boundary between the amplitude increase and decrease in the phase plane of t_i/t_c and $\mu_{\mathrm{ph}}/k_B T$. The successful prediction of the phase boundary further verifies the stable amplitude given by Eq. (A7).

Now let us use the scaling analysis to examine the oscillation behavior of the two hydrogel beams in the experiment. The inertia timescale, $t_i = \sqrt{\rho AL^4/EI}$, can be calculated as 0.51 s for the thick beam and 0.82 s for the

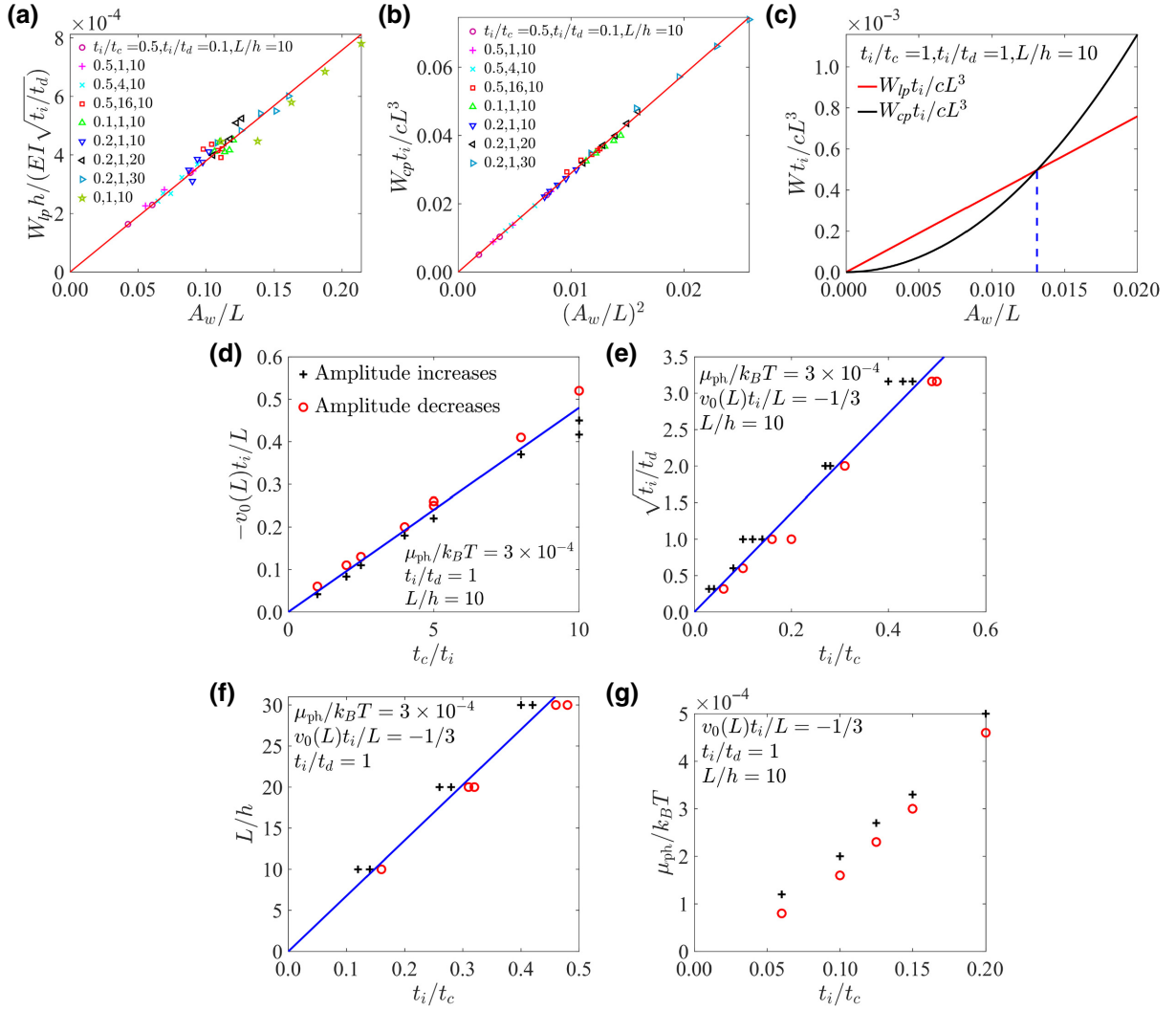FIG. 4. (a) Normalized work done, $W_{lp}h/(EI\sqrt{t_i/t_d})$, as a function of normalized tip amplitude A_w/L; (b) normalized damping energy, $W_{cp}t_i/cL^3$, as a function of the square of the tip amplitude, $(A_w/L)^2$, for a wide range of t_i/t_c, t_i/t_d, and L/h. (c) Normalized work input and energy dissipation as a function of normalized tip amplitude A_w/L. Boundaries between amplitude increase and decrease in phase planes of different dimensionless parameters: (d) in the phase plane of t_c/t_i and $v_0(L)t_i/L$ under constant μ_{ph}/k_BT, t_i/t_d, and L/h; (e) in the phase plane of t_i/t_c and $\sqrt{t_i/t_d}$ under constant μ_{ph}/k_BT, $v_0(L)t_i/L$, and L/h; (f) in the phase plane of t_i/t_c and L/h under constant μ_{ph}/k_BT, $v_0(L)t_i/L$, and t_i/t_d; (g) in the phase plane of t_i/t_c and μ_{ph}/k_BT under constant $v_0(L)t_i/L$, t_i/t_d, and L/h. All symbols are numerical results, and lines are fitting results from the scaling analysis.

thin beam, given $\rho = 10^3$ kg/m^3. The corresponding frequencies can be approximated as $\omega \approx 3.5/t_i = 6.84$ and 4.26 rad/s, respectively. These values agree with the experimentally observed frequencies of 6.28 and 1.19 rad/s, indicating that simplification of the hydrogels as cantilever beams vibrating in the first mode is reasonable. The deviation is because in the experiment the end of a horizontal hydrogel is not fixed, but connected to a vertical portion of the hydrogel, which has the freedom to vibrate itself; a thinner hydrogel pillar corresponds to a weaker boundary constraint, and therefore, a lower frequency. To further estimate the viscous relaxation timescale, t_c, in experiments, we approximate the damping coefficient, c,

to be 4.45×10^{-3} Pa s (Appendix D) and, as a result, $t_c = \rho A/c = 0.14$ s for the thick beam and $t_c = 0.055$ s for the thin beam. By using the diffusivity of our hydrogel, $D = 10^{-8}$ m^2/s, we can calculate $t_d = h^2/D = 81$ s for the thick beam and $t_d = 31.36$ s for the thin beam. Consequently, the normalized diffusivity, t_i/t_d, is 6.3×10^{-3} and the normalized damping factor, t_i/t_c, is 3.58 for the thick beam, while $t_i/t_d = 2.62 \times 10^{-2}$ and $t_i/t_c = 14.86$ for the thin beam. The length-to-thickness ratios for the thick and thin beams in experiments are $L/h = 18.9$ and 30.4, respectively. The spontaneous photostrain on the surface exposed to light, $\varepsilon_0 = f(\mu_{ph}/k_BT)$ (Appendix C), for PNIPAAm hydrogels can be estimated as 0.2. Using Eq.
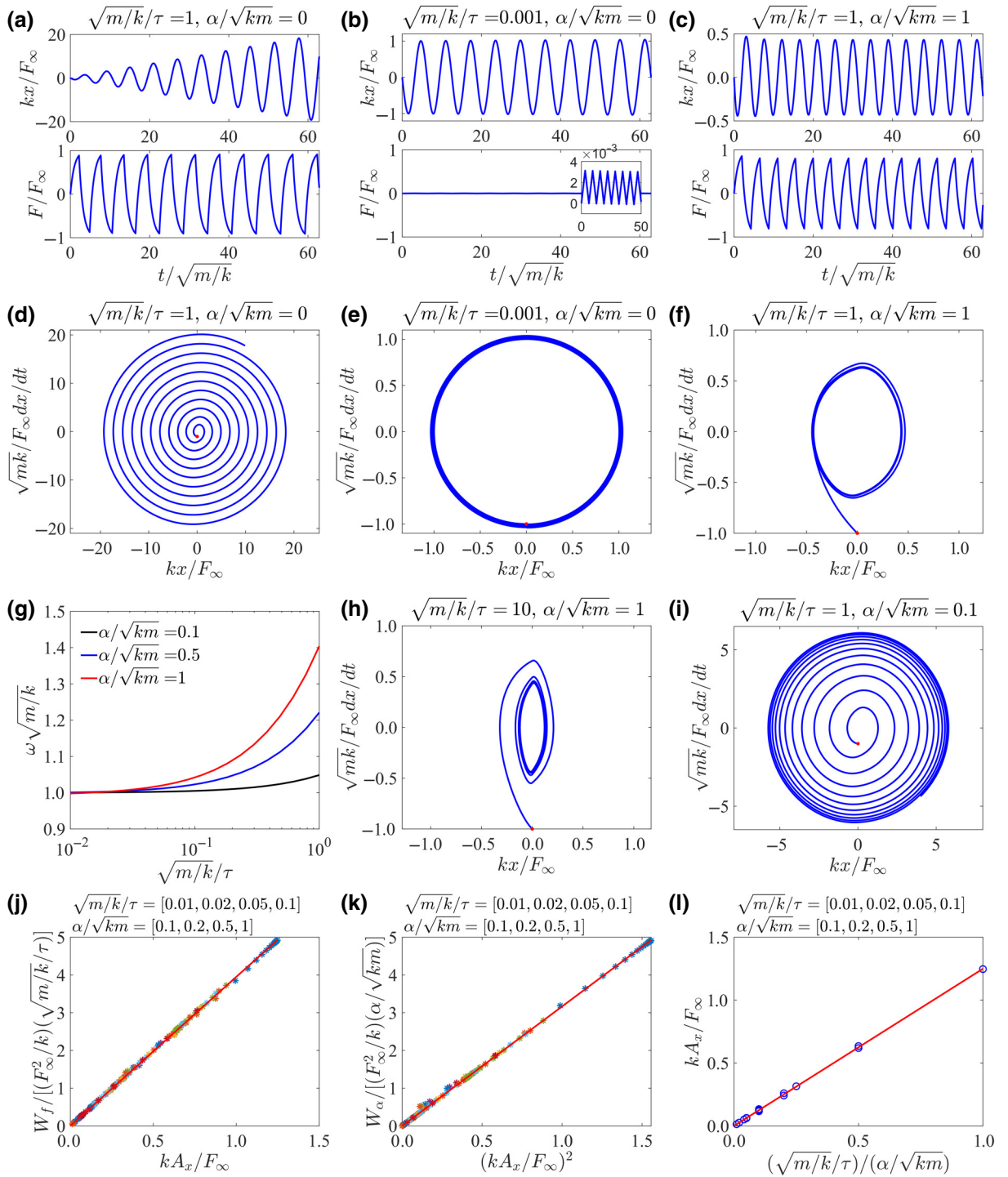
FIG. 5. (a),(b) Undamped time response of displacement and excitation force for timescale ratios $\sqrt{m/k}/\tau = 1$ and $\sqrt{m/k}/\tau = 0.001$, respectively. (d),(e) Undamped phase plane for timescales $\sqrt{m/k}/\tau = 1$ and $\sqrt{m/k}/\tau = 0.001$, respectively. (c) Damped time response of displacement and excitation force. (f),(h),(i) Damped phase plane for different normalized excitation velocities and damping factors. (g) Dependence of vibration frequency $\omega\sqrt{m/k}$ on normalized excitation velocity $\sqrt{m/k}/\tau$ under different normalized damping factors $\alpha/\sqrt{km}$. (j) Normalized work done as a function of normalized vibration amplitude; (k) normalized damping energy as a function of the square of vibration amplitude for a wide range of $\sqrt{m/k}/\tau$ and $\alpha/\sqrt{km}$. (l) Normalized stable amplitude as a function of the ratio between excitation velocity $\sqrt{m/k}/\tau$ and normalized damping factors $\alpha/\sqrt{km}$. In (j)–(l), all symbols are numerical results under different combinations of data sets $\sqrt{m/k}/\tau = [0.01, 0.02, 0.05, 0.1]$ and $\alpha/\sqrt{km} = [0.1, 0.2, 0.5, 1]$, and lines are fitting results from the scaling analysis.

(8), we can calculate that the normalized stable amplitudes, $f\left(\mu_{\mathrm{ph}}/k_B T\right)\frac{L}{h}\frac{\sqrt{t_i/t_d}}{t_i/t_c}$, are comparable for the thick and thin beams and are 0.084 and 0.066, respectively. However, as their normalized initial amplitudes, $v_0(L)t_i/L$, are very different, 0.12 and 9.7×10^{-3} for the thick and thin beams, respectively, this explains why we observe an amplitude decrease in the thick beam and an amplitude increase in the thin beam. Notably, a prefactor is needed on the right-hand side of the scaling relation in Eq. (8) to equate the initial amplitude to the stable amplitude. The prefactor obtained from our numerical calculation is about 0.1, which makes the stable amplitude of the thin beam slightly smaller than that of the initial amplitude. Considering the simplicity of the scaling analysis, we can still claim its success in predicting the amplitude variation of the self-excited oscillation. Since damping from water is high, it is usually challenging to observe autonomous vibration of hydrogels in water. In our experiments, the relatively high diffusivity of water in the hydrogels is the enabling factor for self-excited oscillation.

F. Mass-spring-damper system with nonsmooth excitation force

We further propose a simplified single-degree-of-freedom mass-spring-damper system to shed light on the various features we observe in the photodriven hydrogel oscillator. Analogous to the photomoment, a position- and time-dependent forcing term, F, is added as an excitation force:

$$m\ddot{x} + \alpha\dot{x} + kx = F,$$
$$\dot{F} = -[F + F_\infty \mathrm{sgn}(x)]/\tau, \tag{9}$$

where m is the mass, α is the damping factor, k is the stiffness of the spring, $\cdot$ denotes time derivative d/dt, F_∞ is an excitation force constant, and $\mathrm{sgn}(x) = |x|/x$. The sgn term, as a nonsmooth piecewise term, mimics the ever-switching light source in the hydrogel system. The excitation force, F, changes exponentially over time, with a characteristic timescale τ, featuring a nonequilibrium process, such as diffusion or reaction. This simplified system, originating from prototypical systems of dynamically shifted oscillators [34–37], serves as a good approximation for us to understand the response-dependent excitation of the hydrogel cantilever. Similar to the hydrogel oscillator, we have three timescales, namely, the viscous relaxation timescale, m/α; the inertia timescale, $\sqrt{m/k}$; and the excitation timescale, τ, which define two timescale ratios, the normalized damping factor, $\alpha/\sqrt{km}$, and the normalized excitation velocity, $\sqrt{m/k}/\tau$.

First consider the ideal scenario where there is no damping, $\alpha = 0$. When the excitation timescale is comparable to the inertia timescale, $\sqrt{m/k}/\tau = 1$, the vibration amplitude increases as a function of time and the trajectory on the phase plane diverges away from the initial position

[Figs. 5(a) and 5(d)]. When the excitation timescale is much larger than the inertia timescale, $\sqrt{m/k}/\tau = 0.001$, the excitation force, F, is very small, and therefore, hardly affects the motion [Fig. 5(b)]. The trajectory on the phase plane is close to a circle [Fig. 5(e)], indicating that the motion is similar to a harmonic oscillation. The amplitude can decrease [Fig. 5(c)] by adding a damping term, $\alpha\dot{x}$, and the trajectory goes to a stable limit cycle on its phase plane [Fig. 5(f)]. The simplified model predicts that a higher normalized damping factor, $\alpha/\sqrt{km}$, or a higher normalized excitation velocity, $\sqrt{m/k}/\tau$, raises the frequency, $\omega\sqrt{m/k}$ [Fig. 5(g)], which is consistent with the prediction of the hydrogel cantilever model. The increase of frequency can be observed from the limit cycle, which changes from circular to oval shaped, where the ratio between the amplitude of velocity and displacement increases [Figs. 5(f), 5(h) and 5(i)].

We further study the work done and damping energy through scaling analysis. When the excitation velocity, $\sqrt{m/k}/\tau$, is limited to less than 0.1, the normalized vabration frequency is almost constant. The work done by the force over a period is $W_f = \int_0^{T_p} F\dot{x}\,dt$ and can be rewritten as $W_f \sim (F_\infty^2/k)\left(\sqrt{m/k}/\tau\right)(kA_x/F_\infty)$, where A_x is the vibration amplitude (Appendix E). The damping energy over a period is $W_\alpha = \int_0^{T_p} \alpha\dot{x}^2\,dt$ and can be rewritten as $W_\alpha \sim (F_\infty^2/k)\left(\alpha/\sqrt{km}\right)(kA_x/F_\infty)^2$ (Appendix E). Numerical results prove that the normalized work, $W_f/\left[(F_\infty^2/k)\left(\sqrt{m/k}/\tau\right)\right]$, is proportional to the normalized amplitude, kA_x/F_∞ [Fig. 5(j)], and the damping energy, $W_\alpha/\left[(F_\infty^2/k)\left(\alpha/\sqrt{km}\right)\right]$, is proportional to the square of the normalized amplitude, $(kA_x/F_\infty)^2$ [Fig. 5(k)]. By equating W_f and W_α, the stable amplitude is obtained as $kA_x/F_\infty \sim \left(\sqrt{m/k}/\tau\right)/\left(\alpha/\sqrt{km}\right)$. Consistent with the prediction, the numerical results show that the stable amplitude is proportional to the excitation velocity and inversely proportional to the damping factor [Fig. 5(l)].

IV. CONCLUSIONS

This paper investigates the mechanism and energy flow of photodriven self-excited hydrogel oscillators, the amplitude of which can increase or decrease with time under constant light radiation. When the hydrogel cantilever oscillates, the light incidence switches between the top and bottom surfaces, inducing a periodic photomoment with the same frequency as that of the oscillation. Since the photomoment is induced by an inhomogeneous distribution of water concentration through the thickness of the cantilever due to a nonequilibrium diffusion process, diffusion kinetics determines the temporal evolution of the photomoment. We find that, when the diffusion timescale is comparable to the inertia timescale, the vibration of the cantilever can reach a significantly high amplitude

and remain stable. By analyzing the work done by radiation, it turns out that the synergy between the photomoment and oscillation ensures that positive photomechanical energy is pumped into the system every cycle to maintain self-excited oscillation, overcoming damping. Based on dimensional analysis, we find that the work input is proportional to the vibration amplitude and the damping energy is proportional to the square of the amplitude. The balance of the work input and the energy dissipation determines the stable amplitude, which turns out to scale with length-to-thickness ratio L/h, square root of normalized diffusivity t_i/t_d, and inverse of normalized damping factor t_i/t_c, and depends on the radiation-induced chemical potential change of water, $\mu_{\mathrm{ph}}/k_B T$. By equating the initial and stable amplitudes, we construct phase diagrams for the increase and decrease of the oscillation amplitude. To further shed light on the self-excited oscillation, a simplified mass-spring-damper system with a single degree of freedom is proposed to understand the major features and energy flow in generalized self-excited oscillating systems. The effect of the material and geometric parameters on the vibration frequency, amplitude, and energy of the hydrogel cantilever can be mostly reproduced by the simplified system. This study elucidates the design requirements of stimuli-responsive self-excited oscillators.

APPENDIX A: THEORY FOR SELF-EXCITED HYDROGEL OSCILLATORS

We model the vibration of a hydrogel cantilever of length L and thickness h in water triggered by constant light radiation in the axial direction [Fig. 1(a)]. The cantilever is assumed to undergo small deflection, $w(x,t)$, as a function of coordinate x and time t, governed by

$$\rho A \frac{\partial^2 w}{\partial t^2} + c \frac{\partial w}{\partial t} + EI \frac{\partial^4 w}{\partial x^4} = EI \frac{\partial^2 (1/R_{\mathrm{ph}})}{\partial x^2}, \quad \text{(A1)}$$

with density ρ, cross-section area A, Young's modulus E, and area moment of inertia I. The second term assumes that the damping force on the unit length of the hydrogel is proportional to the deflection velocity, with damping

coefficient c, due to the drag from water. The term on the right-hand side of Eq. (A1) is the distributed load produced by photomoment EI/R_{ph}, where R_{ph} is the spontaneous radius of curvature in the region $x \in [0, d_{\mathrm{ph}}]$, with the width of the light beam, d_{ph}, arising from a gradient of photodriven deformation through the thickness yet to be determined by solving the diffusion equation of water molecules. With the left end clamped and the right end free, the boundary conditions are

$$w(0,t) = \frac{\partial w}{\partial x}(0,t) = 0, \ \frac{\partial^2 w}{\partial x^2}(L,t) = \frac{\partial^3 w}{\partial x^3}(L,t) = 0. \quad \text{(A2)}$$

We model the diffusion of water molecules driven by a gradient of its chemical potential. The free energy density of a hydrogel consists of an elastic part and a mixing part, $W(\mathbf{F}, C) = W_{\mathrm{net}}(\mathbf{F}) + W_{\mathrm{mix}}(C)$. The elastic part considers the elastic energy of the polymer network as a function of the deformation gradient, $\mathbf{F}$, per volume in the reference dry state [43,44]:

$$W_{\mathrm{net}}(\mathbf{F}) = \frac{1}{2} N k_B T [\mathrm{tr}(\mathbf{F}\mathbf{F}^T) - 3 - 2 \log(\det \mathbf{F})], \quad \text{(A3)}$$

where N is the cross-link density of the hydrogel, k_B is the Boltzmann constant, and T is the temperature. The mixing energy density between the polymer and water per reference volume is a function of the water concentration, C, namely, the number of water molecules per unit reference volume [45]:

$$W_{\mathrm{mix}}(C) = k_B T C \left[\log \left(\frac{\Omega C}{1 + \Omega C} \right) + \frac{\chi}{1 + \Omega C} \right], \quad \text{(A4)}$$

where Ω is the volume of a water molecule, and χ is the Flory-Huggins interaction constant between the polymer and water. Both the polymer network and water are assumed to be incompressible, so the volume change of the hydrogel is purely due to the migration of water molecules, $J = \det(\mathbf{F}) = \Omega C + 1$. The chemical potential of water molecules in the hydrogel, μ, can be calculated by [38]

$$\mu = \frac{\partial W}{\partial C} + \Pi \Omega, \quad \text{(A5)}$$

where Π is the osmotic pressure, as determined by the boundary conditions. When the hydrogel freely swells in water without constraints, the Cauchy stress,

$$\boldsymbol{\sigma} = (\partial W / \partial \mathbf{F}) \mathbf{F}^T / J - \Pi \mathbf{I}, \quad \text{(A6)}$$

is zero, i.e., $\boldsymbol{\sigma} = 0$, and the osmotic pressure can be determined as $\Pi_0 = N k_B T (\lambda_0^{-1} - \lambda_0^{-3})$, where λ_0 is the equilibrium isotropic stretch ratio with respect to the dry state, relating to the water concentration, C_0, by $\lambda_0 =$

$(1 + \Omega C_0)^{1/3}$. The equilibrium water concentration, C_0, can be determined by $\mu(C_0) = 0$ using Eq. (A5), i.e., the chemical potential of water in the hydrogel equals that of pure water outside the hydrogel.

Absorption of light raises the temperature of the hydrogel on the irradiated surface, increasing the chemical potential of the water molecules, driving the water molecules to diffuse out of the hydrogel. Since the cantilever length is much larger than its thickness, water diffusion in the length direction can be neglected. We model the photothermally driven water migration as a one-dimensional diffusion problem along the thickness, with Z as the reference coordinate in the thickness direction [38,39]:

$$\dot{C} = \nabla \cdot (\mathbf{M} \cdot \nabla \mu), \qquad (A7)$$

where $\mathbf{M}$ is the mobility tensor of water molecules in the hydrogel. To capture that the water molecules diffuse out of the hydrogel through the illuminated surface, we simply assume that light changes the chemical potential of the water molecules on the illuminated boundary, i.e., apply $\mu = -\mu_{\text{ph}} < 0$ on the illuminated surface and $\mu = 0$ on the nonilluminated surface.

Next, we decompose the total deformation gradient, $\mathbf{F}$, into $\mathbf{F} = \mathbf{F}'\mathbf{F}_0$, where $\mathbf{F}_0 = \text{diag}(\lambda_0, \lambda_0, \lambda_0)$ maps the dry configuration to the wet nonirradiated one, and $\mathbf{F}'$ maps the wet nonirradiated configuration to the current irradiated configuration. We assume that the deformation arising from the swelling of the hydrogel with respect to the dry configuration is finite, while the deformation of oscillation under light radiation can be considered small. With linearized strain $\boldsymbol{\varepsilon} = (\mathbf{F}' + \mathbf{F}'^T)/2 - \mathbf{I}$, the Cauchy stress, $\boldsymbol{\sigma}$, Eq. (A6), can be linearized as

$$\boldsymbol{\sigma} = \frac{2Nk_BT}{\lambda_0}\boldsymbol{\varepsilon} + [\Pi_0(1 - \text{tr}\boldsymbol{\varepsilon}) - \Pi]\mathbf{I}. \qquad (A8)$$

Then diffusion Eq. (A7) can be rewritten as

$$\frac{\partial C}{\partial t} = \frac{D}{k_BT}\frac{\partial}{\partial z}\left(\frac{C}{\lambda_z^2}\frac{\partial \mu}{\partial z}\right), \qquad (A9)$$

where $\lambda_z = 1 + \varepsilon_z$ is the z component of $\mathbf{F}'$ after linearization, and D is the diffusivity of the water molecules in the hydrogel. Photodriven diffusion induces spontaneous photostrain, $\boldsymbol{\varepsilon}_{\text{ph}}(z) = \text{diag}[\varepsilon_{\text{ph}}(z), \varepsilon_{\text{ph}}(z), \varepsilon_{\text{ph}}(z)]$, as a function of position z, where $\varepsilon_{\text{ph}}(z) < 0$. We assume that the hydrogel undergoes pure bending with respect to the nonirradiated state. Since the total volume change is due to diffusion, we have $\text{tr}\boldsymbol{\varepsilon} = \text{tr}\boldsymbol{\varepsilon}_{\text{ph}} \doteq (\Omega C + 1)/(\Omega C_0 + 1) - 1$, namely, $\varepsilon_{\text{ph}}(z) \doteq \{[\Omega C(z) + 1]/(\Omega C_0 + 1) - 1\}/3$. Based on pure bending, the total strain should be diagonal in its principal axes, $\boldsymbol{\varepsilon}(z) = \text{diag}[\varepsilon_x(z), \varepsilon_y(z), \varepsilon_z(z)]$, where $\varepsilon_x(z)$ can be deemed linear in z, having a neutral plane at

z_n, namely, $\varepsilon_x(z) = (z_n - z)/R$, with R the radius of curvature of the beam. We will show how to determine z_n using mechanical equilibrium hereafter. When diffusion just starts, there could be an infinitesimal curvature along the y direction alongside the x curvature, but it will be easily suppressed by the dominant curvature, $1/R$, as its magnitude develops [46]. Assuming there is no stress along y and z, we can solve for $\varepsilon_y = \varepsilon_z = [\text{tr}\boldsymbol{\varepsilon}_{\text{ph}} - (z_n - z)/R]/2$, and the osmotic pressure, $\Pi = (Nk_BT/\lambda_0)(\text{tr}\boldsymbol{\varepsilon} - \varepsilon_x) + \Pi_0(1 - \text{tr}\boldsymbol{\varepsilon})$. Inserting Π into Eq. (A8), we can determine the only nonvanishing stress component along x,

$$\sigma_x = \frac{3Nk_BT}{\lambda_0}\left(\frac{z_n - z}{R} - \varepsilon_{\text{ph}}\right). \qquad (A10)$$

Using the relationship, $E = 3Nk_BT/\lambda_0$, between the Young's modulus and cross-link density, we can see that Eq. (A10) is reminiscent of the one-dimensional classical stress-strain relationship in the presence of a thermal strain, except the prefactor associated with preradiation swelling. Applying the force-free to Eq. (A10), namely, $\int_A \sigma_x dA = 0$ and $\int_A \sigma_x z dA = 0$, we get $z_n/R = \int_A \varepsilon_{\text{ph}}(z)dA/A$. Then we calculate the internal moment using Eq. (A10),

$$\int_A \sigma_x z dA = EI(1/R - 1/R_{\text{ph}}), \qquad (A11)$$

with

$$1/R_{\text{ph}} = -\int_A \varepsilon_{\text{ph}}(z)z dA/I, \qquad (A12)$$

where we take the centroid of the cross section as the origin of the coordinate system.

APPENDIX B: TIME RESPONSE OF THE CANTILEVER'S TIP DISPLACEMENT AND PHOTOCURVATURE FOR $t_i/t_d = 100\,000$

As shown in Fig. 6, when the diffusion is much faster than the vibration, the photocurvature acts like a step-function excitation.

APPENDIX C: SCALING OF THE RADIUS OF CURVATURE OF A HYDROGEL OSCILLATOR

To estimate the radius of curvature of a hydrogel oscillator due to an inhomogeneous water concentration along the thickness, we simply consider that water diffuses up to certain diffusion distance, $h_d \sim \sqrt{DT_p}$, where D is the diffusivity of water molecules in the hydrogel and T_p is the period of the vibration. The spontaneous photostrain is assumed to be ε_0 on the shined surface, $z = h/2$, which linearly decreases with z, and reaches zero at $z = h/2 - h_d$,

i.e.,

$$\varepsilon_{\text{ph}}(z) \sim \frac{\varepsilon_0}{h_d}\left[z - \left(\frac{h}{2} - h_d\right)\right], \quad h/2 - h_d < z < h/2,$$
(C1)

Using Eq. (3), we have

$$1/R_{\text{ph}} = -\int_A \varepsilon_{\text{ph}}(z)z\,dA/I \sim \int_{\frac{h}{2}-h_d}^{\frac{h}{2}} \frac{\varepsilon_0}{h_d}\frac{1}{h^3}$$

$$\left[z - \left(\frac{h}{2} - h_d\right)\right]z\,dz \sim \frac{\varepsilon_0 h_d}{h^2} \sim \frac{\varepsilon_0\sqrt{DT_p}}{h^2}, \quad (\text{C2})$$

where ε_0 is determined by the photochemical potential, $\mu_{\text{ph}}/k_B T$, and we assume $h_d < h$. Therefore, the spontaneous radius of curvature scales with the square of the thickness, $R_{\text{ph}} \sim h^2$, is inversely proportional to the diffusion thickness, $\sqrt{DT_p}$, and nonlinearly depends on the photochemical potential, $\mu_{\text{ph}}/k_B T$.

APPENDIX D: ESTIMATION OF THE DAMPING COEFFICIENT

For a slender structure with length L and width b, vibrating with velocity v, the Reynolds number can be calculated as Re $= \rho_w v b/\mu_w$. Given the density of water, $\rho_w = 10^3$ kg/m^3; viscosity of water, $\mu_w = 8.9 \times 10^{-4}$ Pa s; $b = 10^{-3}$ mm; and velocity $v = 10^{-3}$ m/s, we know that the fluid has a low Reynold number, Re ≈ 1. The damping coefficient, c, can be calculated from the drag force, F_d: $c = F_d/Lv$. For a low-Reynolds-number fluid, the drag
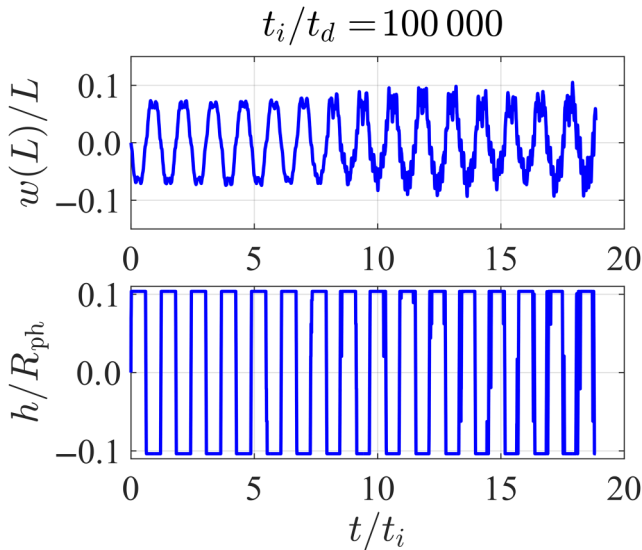

FIG. 6. Time response of the cantilever's tip displacement and photocurvature for normalized diffusivity $t_i/t_d = 100\,000$. Curvature behaves like a step function. Frequency is higher than that with a smaller normalized diffusivity.

coefficient defined as $c_d = 2F_d/\rho_w v^2 Lb$ equals A_d/Re, with A_d as a constant coefficient, depending on the cross section of the slender structure [47]. Therefore, the damping coefficient is calculated as $c = A_d\mu_w/2$. When the cross section is circular, A_d is 24. Here, we just generically set A_d to 10. Therefore, the damping coefficient is estimated to be 4.45×10^{-3} Pa s.

APPENDIX E: SCALING OF THE WORK DONE AND DAMPING ENERGY OF THE MASS-SPRING-DAMPER SYSTEM

When the excitation velocity, $\sqrt{m/k}/\tau$, is limited to less than 0.1, the normalized vabriation frequency is almost a constant. Using Eq. (9), the maximum applied force, $F_{\max}$, is proportional to $F_\infty\sqrt{m/k}/\tau$, namely, $F_{\max} \sim F_\infty\sqrt{m/k}/\tau$. Therefore, we have

$$W_f = \int_0^{T_p} F\dot{x}\,dt \sim F_{\max}A_x \sim (F_\infty^2/k)\left(\sqrt{m/k}/\tau\right)$$

$$(kA_x/F_\infty).$$
(E1)

The damping energy is obtained as

$$W_\alpha = \int_0^{T_p} \alpha\dot{x}^2\,dt \sim \alpha\frac{A_x^2}{T_p} \sim \alpha\frac{A_x^2}{\sqrt{m/k}}$$

$$\sim (F_\infty^2/k)\left(\alpha/\sqrt{km}\right)(kA_x/F_\infty)^2.$$
(E2)

[1] M. A. C. Stuart, W. T. Huck, J. Genzer, M. Müller, C. Ober, M. Stamm, G. B. Sukhorukov, I. Szleifer, V. V. Tsukruk, and M. Urban, Emerging applications of stimuli-responsive polymer materials, Nat. Mater. **9**, 101 (2010).

[2] M. Rogóż, H. Zeng, C. Xuan, D. S. Wiersma, and P. Wasylczyk, Light-driven soft robot mimics caterpillar locomotion in natural scale, Adv. Opt. Mater. **4**, 1689 (2016).

[3] G. Li, X. Chen, F. Zhou, Y. Liang, Y. Xiao, X. Cao, Z. Zhang, M. Zhang, B. Wu, and S. Yin, Self-powered soft robot in the Mariana Trench, Nature **591**, 66 (2021).

[4] Y. Kim, H. Yuk, R. Zhao, S. A. Chester, and X. Zhao, Printing ferromagnetic domains for untethered fast-transforming soft materials, Nature **558**, 274 (2018).

[5] H. Shahsavan, A. Aghakhani, H. Zeng, Y. Guo, Z. S. Davidson, A. Priimagi, and M. Sitti, Bioinspired underwater locomotion of light-driven liquid crystal gels, Proc. Natl. Acad. Sci. **117**, 5125 (2020).

[6] L. Hines, K. Petersen, G. Z. Lum, and M. Sitti, Soft actuators for small-scale robotics, Adv. Mater. **29**, 1603483 (2017).

[7] Y. Zhao, C. Xuan, X. Qian, Y. Alsaid, M. Hua, L. Jin, and X. He, Soft phototactic swimmer based on self-sustained hydrogel oscillator, Sci. Robot. **4**, eaax7112 (2019).

[8] Y. Kim, J. van den Berg, and A. J. Crosby, Autonomous snapping and jumping polymer gels, Nat. Mater. **20**, 1695 (2021).

[9] K. Li, X. Su, and S. Cai, Self-Sustained rolling of a thermally responsive Rod on a Hot surface, Extreme Mech. Lett. **42**, 101116 (2021).

[10] H. Zeng, M. Lahikainen, L. Liu, Z. Ahmed, O. M. Wani, M. Wang, H. Yang, and A. Priimagi, Light-fuelled freestyle self-oscillators, Nat. Commun. **10**, 5057 (2019).

[11] Z.-Z. Nie, B. Zuo, M. Wang, S. Huang, X.-M. Chen, Z.-Y. Liu, and H. Yang, Light-driven continuous rotating möbius strip actuators, Nat. Commun. **12**, 2334 (2021).

[12] H. Zhu, B. Xu, Y. Wang, X. Pan, Z. Qu, and Y. Mei, Self-powered locomotion of a hydrogel water strider, Sci. Robot. **6**, eabe7925 (2021).

[13] K. Korner, A. S. Kuenstler, R. C. Hayward, B. Audoly, and K. Bhattacharya, A nonlinear beam model of photomotile structures, Proc. Natl. Acad. Sci. **117**, 9762 (2020).

[14] L. Yang, L. Chang, Y. Hu, M. Huang, Q. Ji, P. Lu, J. Liu, W. Chen, and Y. Wu, An autonomous soft actuator with light-driven self-sustained wavelike oscillation for phototactic self-locomotion and power generation, Adv. Funct. Mater. **30**, 1908842 (2020).

[15] Z. Hu, Y. Li, and J. Lv, Phototunable self-oscillating system driven by a self-winding fiber actuator, Nat. Commun. **12**, 3211 (2021).

[16] T. J. White, N. V. Tabiryan, S. V. Serak, U. A. Hrozhyk, V. P. Tondiglia, H. Koerner, R. A. Vaia, and T. J. Bunning, A high frequency photodriven polymer oscillator, Soft Matter **4**, 1796 (2008).

[17] X. He, M. Aizenberg, O. Kuksenok, L. D. Zarzar, A. Shastri, A. C. Balazs, and J. Aizenberg, Synthetic homeostatic materials with chemo-mechano-chemical self-regulation, Nature **487**, 214 (2012).

[18] A. W. Hauser, S. Sundaram, and R. C. Hayward, Photothermocapillary Oscillators, Phys. Rev. Lett. **121**, 158001 (2018).

[19] P. R. Buskohl and R. A. Vaia, Belousov-zhabotinsky autonomic hydrogel composites: Regulating waves via asymmetry, Sci. Adv. **2**, e1600813 (2016).

[20] A. Chakrabarti, G. P. T. Choi, and L. Mahadevan, Self-Excited Motions of Volatile Drops on Swellable Sheets, Phys. Rev. Lett. **124**, 258002 (2020).

[21] R. K. Manna, O. E. Shklyaev, and A. C. Balazs, Chemical pumps and flexible sheets spontaneously form self-regulating oscillators in solution, Proc. Natl. Acad. Sci. **118**, e2022987118 (2021).

[22] S. Maeda, Y. Hara, T. Sakai, R. Yoshida, and S. Hashimoto, Self-walking Gel, Adv. Mater. **19**, 3480 (2007).

[23] R. Yoshida and T. Ueki, Evolution of self-oscillating polymer gels as autonomous polymer systems, NPG Asia Mater. **6**, e107 (2014).

[24] B. E. Treml, R. N. McKenzie, P. Buskohl, D. Wang, M. Kuhn, L.-S. Tan, and R. A. Vaia, Autonomous motility of polymer films, Adv. Mater. **30**, 1705616 (2018).

[25] D. Corbett, C. Xuan, and M. Warner, Deep optical penetration dynamics in photobending, Phys. Rev. E **92**, 013206 (2015).

[26] A. H. Gelebart, G. Vantomme, E. W. Meijer, and D. J. Broer, Mastering the photothermal effect in liquid crystal networks: A general approach for self-sustained mechanical oscillators, Adv. Mater. **29**, 1606712 (2017).

[27] K. Kumar, C. Knie, D. Bleger, M. A. Peletier, H. Friedrich, S. Hecht, D. J. Broer, M. G. Debije, and A. P. Schenning,

A chaotic self-oscillating sunlight-driven polymer actuator, Nat. Commun. **7**, 11975 (2016).

[28] S. Serak, N. Tabiryan, R. Vergara, T. J. White, R. A. Vaia, and T. J. Bunning, Liquid crystalline polymer cantilever oscillators fueled by light, Soft Matter **6**, 779 (2010).

[29] K. M. Lee, M. L. Smith, H. Koerner, N. Tabiryan, R. A. Vaia, T. J. Bunning, and T. J. White, Photodriven, flexural–torsional oscillation of glassy azobenzene liquid crystal polymer networks, Adv. Funct. Mater. **21**, 2913 (2011).

[30] A. H. Gelebart, D. Jan Mulder, M. Varga, A. Konya, G. Vantomme, E. W. Meijer, R. L. B. Selinger, and D. J. Broer, Making waves in a photoactive polymer film, Nature **546**, 632 (2017).

[31] K. Li and S. Cai, Modeling of light-driven bending vibration of a liquid crystal elastomer beam, J. Appl. Mech. **83**, 031009 (2016).

[32] G. Vantomme, A. H. Gelebart, D. J. Broer, and E. W. Meijer, Self-sustained actuation from heat dissipation in liquid crystal polymer networks, J. Polym. Sci., Part A: Polym. Chem. **56**, 1331 (2018).

[33] D. Zhao and Y. Liu, Photomechanical vibration energy harvesting based on liquid crystal elastomer cantilever, Smart Mater. Struct. **28**, 075017 (2019).

[34] O. Makarenkov and J. S. Lamb, Dynamics and bifurcations of nonsmooth systems: A survey, Phys. Nonlinear Phenom. **241**, 1826 (2012).

[35] W. M. Hartmann, The dynamically shifted oscillator, Am. J. Phys. **54**, 28 (1986).

[36] Y. Chen and L. Jin, Snapping-Back buckling of wide hyperelastic columns, Extreme Mech. Lett. **34**, 100600 (2019).

[37] A. Li, L. Ma, D. Keene, J. Klingel, M. Payne, and X. Wang, Forced oscillations with linear and nonlinear damping, Am. J. Phys. **84**, 32 (2016).

[38] W. Hong, X. Zhao, J. Zhou, and Z. Suo, A theory of coupled diffusion and large deformation in polymeric gels, J. Mech. Phys. Solids **56**, 1779 (2008).

[39] C. Xuan and L. Jin, Concurrent reaction and diffusion in photo-responsive hydrogels, J. Mech. Phys. Solids **124**, 599 (2019).

[40] A. Mourran, H. Zhang, R. Vinokur, and M. Möller, Soft microrobots employing nonequilibrium actuation via plasmonic heating, Adv. Mater. **29**, 1604825 (2017).

[41] See the Supplemental Material at http://link.aps.org/supplemental/10.1103/PhysRevApplied.17.014007 for videos exhibiting photodriven self-excited hydrogel oscillators with increasing and decreasing amplitude.

[42] J. P. Den Hartog, *Mechanical Vibrations* (McGraw-Hill, New York, 1956).

[43] P. J. Flory and J. Rehner Jr, Statistical mechanics of crosslinked polymer networks I. Rubberlike elasticity, J. Chem. Phys. **11**, 512 (1943).

[44] P. J. Flory, *Principles of Polymer Chemistry* (Cornell University Press, Ithaca, NY, 1953).

[45] P. J. Flory, Thermodynamics of high polymer solutions, J. Chem. Phys. **10**, 51 (1942).

[46] M. Warner, C. D. Modes, and D. Corbett, Suppression of curvature in nematic elastica, Proc. R. Soc. Math. Phys. Eng. Sci. 466, 3561 (2010).

[47] A. M. Jones and J. G. Knudsen, Drag coefficients at low reynolds numbers for flow past immersed bodies, AIChE J. **7**, 20 (1961).